RESEARCH PAPER

Stiffener layout optimization of plate and shell structures for buckling problem by adaptive growth method

Xiaohu Dong[1] · Xiaohong Ding[1] · Guojie Li[2] · Gareth Peter Lewis[3]

Abstract

Under axial pressure or shear load, thin-walled plate and shell structures are easily destroyed by buckling. This paper presents the design method for finding the optimal stiffener layout on thin-walled plate and shell structures against the buckling by using the adaptive growth method (AGM), which is based on the growth mechanism of branch systems in nature. Firstly, a mathematical model for optimization of the stiffener layout against buckling is established, and a Karush-Kuhn-Tucker (KKT)-based iteration formula is derived. Next, the stiffeners grow or degenerate from "seeds" according to the adaptive growth principle. Several examples, including imperforated and perforated rectangular plates with unilateral axial pressure and shear loading, are demonstrated to validate the effectiveness of the suggested method, and well-defined stiffener layouts are obtained. The results show that the stiffener layout is clear, and the buckling resistance performance of the optimized stiffened structures is greatly improved.

Keywords Stiffener layout optimization · Buckling resistance · Adaptive growth method · Thin-walled plates

1 Introduction

Stiffened plate and shell structures have been widely applied to aerospace, marine, automotive, and other industries because of their lightweight construction. Under axial pressure or shear load, buckling is one of the main failure forms of these structures. To obtain better buckling resistance, the optimum layout of stiffeners on the thin-walled plate and shell structure is of critical significance. In recent years, many research works have focused on finding the optimal geometry and position of stiffeners to improve structural buckling performance. With respect to the patch loading longitudinally stiffened webs problem, Cevik (2007), Cevik et al. (2010) studied the optimum size of longitudinally stiffened webs based on an

existing database of previous experimental tests by genetic programming and stepwise regression. Maiorana et al. (2011) applied different typologies of stiffeners on stiffened plates and gave new practical insights about the shape and optimum position of longitudinal stiffener in webs under axial force in-plane bending or shear act. Chacon et al. (2013a, b, 2014, 2017) and Carlos (2015) discussed the influence of transverse stiffener of steel girders subjected to patch loading by experimental and numerical studies. Nelson et al. (2017) revealed the effect of the compressive load length and the relative position and size of the stiffeners on the ultimate strength. Wang et al. (2014) proposed a two-stage computational framework for cylindrical or flat stiffened panels under uniform or non-uniform axial compression, which contained size and layout optimization of stiffened panels simultaneously. Cheng and Xu (2016) considered two-scale topology optimization of maximum out-of-plane global buckling load factor of stiffened or porous plates subjected to volume constraints on both the macroplate and the microbase cell. To simplify the analysis and to enable the gradient-based optimization, the numerical implementation of the asymptotic homogenization method (NIAH) was introduced. In regard to the shear buckling, Alinia (2005) analyzed 1200 plates subjected to shear loading in order to study the role of stiffeners and to come up with some limits for an optimized design procedure by using ANSYS finite element method of analysis.

✉ Xiaohong Ding
dingxhsh021@126.com

[1] School of Mechanical Engineering, University of Shanghai for Science and Technology, Shanghai 200093, China

[2] Applied Technology College, Soochow University, Suzhou 215325, China

[3] The Sino-British College, University of Shanghai for Science and Technology, Shanghai 200031, China

Subsequently, they gave more details about the shear investigation (Alinia et al. 2007, 2008). Pavlovcic et al. (2007a, b) numerically and experimentally investigated the shear strength of steel plate with trapezoidal stiffeners, and the optimal position of stiffeners was studied. Alinia and Moosavi (2009) and Issa-El-Khoury et al. (2016) also investigated the buckling characteristic of web plates having a longitudinal stiffener in different positions under simultaneous shear and in-plane bending. Conversely, because the presence of holes is often indispensable in many engineering fields, such as maintenance or inspection cutouts in a ship hull, many research works discuss the ultimate strength characteristics of plate and shell structures considering the presence of holes. Paik (2007, 2008) and Komur and Sonmez (2015) gave the ultimate strength characteristics of perforated steel plates under combined biaxial compression and edge shear loads. In addition, Mohammadzadeh et al. (2018) conducted similar research to explore the effects of having the hole in the plate. Shimoda et al. (2016) developed a shape optimization process based on a free-form optimization method to optimize a shell structure with holes under out-of-plane and in-plane shape variations in order to tackle the linear elastic buckling problem. Hao et al. (2016, 2018) studied shape optimization of curvilinear stiffeners around multicutouts. However, most of the abovementioned literature dealt with the size and shape optimization of plate and shell structures, because of the complexity of directly adopting topology optimization. Although the method in these literatures can result in optimal stiffener layout with cutouts structures, the stiffener layout strongly depends on the initial design.

Bendsoe and Sigmund (2003) and Neves et al. (1995) used Solid Isotropic Material with Penalization (SIMP) method to address the stability issues. Manickarajah et al. (1995, 1998) applied the evolutionary structural optimization (ESO) method for optimization of plate buckling resistance, and the optimum thickness distribution of plates that satisfies the prescribed buckling load constraint was obtained. Butler et al. (2001) considered optimum panel design using VICONOPT, which is a fast-running optimization package based on linear eigenvalue buckling theory, and they designed corresponding experiments to identify the buckling modes. Kasaiezadeh et al. (2010) used the level set method (LSM) to maximize the critical buckling load in the topology optimization of engineering structures. Luo and Tong (2015) presented a novel formulation for maximizing linear buckling loads with additional constraints on load-path continuity and lower bound of eigenvalue and investigated topology design optimization of thin-walled structures using a moving isosurface threshold (MIST) method. Gao and Ma (2015) developed two-phase optimization algorithms for minimization of structural compliance considering constraints of volume and buckling load factors, which based on the eigenvalue shift and pseudomode identification. Ye et al. (2017a, b) established a

model of topology optimization with linear buckling constraints based on the independent and continuous mapping (ICM) method to minimize the structure weight and investigated the buckling topology optimization of orthotropic plate and shell structures. Wang et al. (2017, 2019) optimized curved stiffener distributions to enhance the grid-stiffened composite structural buckling resistance. Wu et al. (2019) proposed multimaterial topology optimization for thermo-mechanical buckling problems. To date, different topology optimization techniques have been put into use to address the stability and buckling issues in engineering structures. However, most of the design results are usually fuzzy and complex, which leads to difficulties in the engineering application. Therefore, it is still necessary to develop new design methods for stiffener layout of thin-walled plate and shell structures against buckling.

Huang et al. (2019) presented an engineering method for optimizing complex structures made of bars, beams, shells, or a combination of those components, involving both size and topology design variables. In order to make the primal problem explicit, a branched multipoint function was constructed to approximate the primal functions. Soon afterward, Chen et al. (2019) used an improved gradient-based two-level approximation (GATA) to deal with the simultaneous optimization of stiffened shells with respect to distribution and sizing. An et al. (2018, 2019) introduced extra discrete and continuous variables related to the existence of stiffeners to study on simultaneous optimization of stacking sequence and stiffener layout of a composite stiffened panel. Compared with other structural topology optimization methods, a simple and effective approach termed as adaptive growth method (AGM) has been put forward by Ding and Yamazaki (2004, 2005), Ji et al. (2014). This method is inspired by the growth mechanism of branch systems in nature and has been applied to the optimum layout design of stiffeners in plate and shell structures to minimize strain energy or to maximize fundamental frequency. The advantages of AGM include the following: (1) The implementation of the method is simple and only a few design parameters are introduced, and (2) the method is valid and highly efficient, and well-defined distribution of the stiffeners can be obtained directly. This paper expands AGM to design the stiffener layout for enhancing the buckling resistance of plate and shell structures. A mathematical model for stiffener layout optimization against buckling is established. The optimal iterative process based on AGM drives the stiffeners growing from "seeds" towards the direction to achieve the best buckling resistance of the plate and shell structures, in which the iterative formula is derived from Karush-Kuhn-Tucker (KKT) optimality criterion. A filtering function is used to solve the mesh-dependent problem. Several typical design examples, including imperforated rectangular plates with different aspect ratios and perforated rectangular plates with different holes under unilateral axial
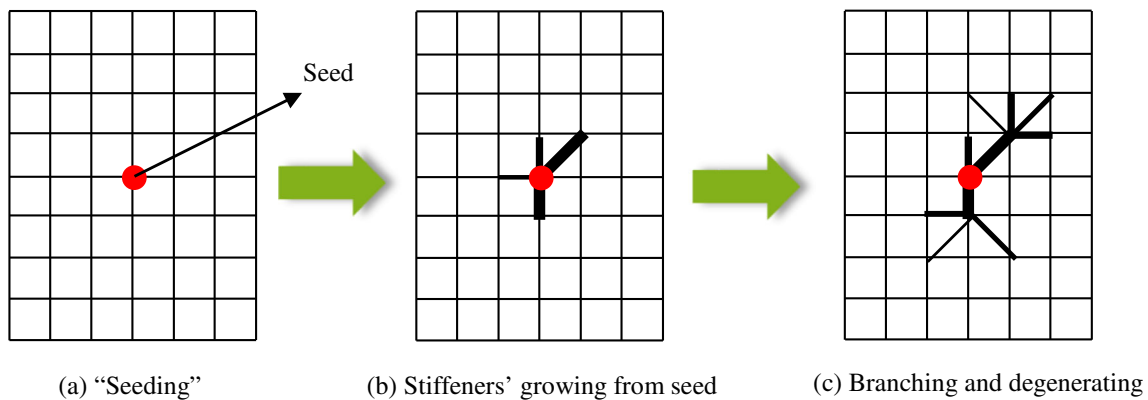
Fig. 1 Adaptive growing and branching process. **a** "Seeding." **b** Stiffeners' growing from seed. **c** Branching and degenerating

pressure or shear loading, are studied, and their design results are discussed and compared with the SIMP method.

The remainder of this paper is organized as follows. In Sect. 2, the design method of adaptive growth method (AGM) is introduced, and a design model for stiffener layout optimization of plate and shell structures against buckling is constructed. Moreover, an iteration formula is derived based on KKT optimum conditions. Several typical design examples, including imperforated and perforated rectangular plates under unilateral axial pressure and shear loading, are studied in Sect. 3, and the obtained well-defined stiffener layouts are discussed. Finally, the main concluding remarks are given in Sect. 4.

2 Design method

2.1 Design method of adaptive growth method

In the natural world, branching systems (e.g., the root system of plants) are controlled by the law of adaptive growth to meet the requirements of the life activities (e.g., geotropism, hydrotropism, and thigmotropism of roots). The adaptive growth method (AGM) was suggested to solve the design problem of the stiffener layout optimization on the basis of the growth

mechanisms of branching systems in nature. As shown in Fig. 1, stiffeners grow from seeds (red point), which are selected according to the loading and supporting conditions. The stiffeners can either grow or degenerate according to their contribution to the design objective. When the stiffeners grow to a certain scale, "branching" will occur, and the stiffeners connected with the "branching points" can participate to grow in the next iteration. The stiffeners are removed if they degenerate to a certain degree. This generate-degenerate process repeats until the convergence conditions are satisfied, and the well-defined distribution of the stiffeners can be obtained.

According to the growth principle of AGM, a ground structure is constructed, which includes two parts, one is plate and the other is stiffener, as shown in Fig. 2. The design domain in Fig. 2a is discretized by four-node shell elements, while two-node beam elements formed by nodes of the corresponding shell elements simulate stiffeners. Thus, each unit consists of one shell element and six beam elements (four beams at four edges and two beams cross in the middle). However, in some cases with complex geometric configurations, there are 3-node triangular elements. In this case, the basic unit contains one triangular shell element and three beam elements, as shown in Fig. 2b. Figure 2c shows the cross section of the stiffened plate structure, where h is the height of the stiffener, and t is the width
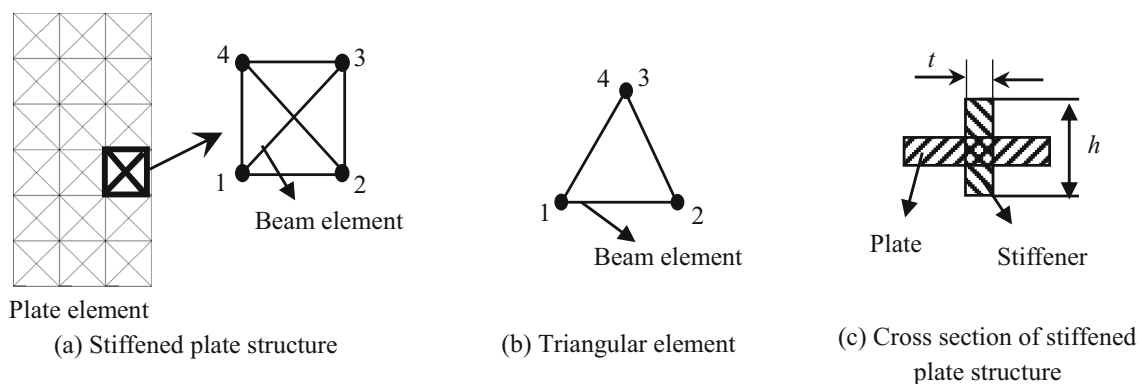

Fig. 2 Ground structure. **a** Stiffened plate structure. **b** Triangular element. **c** Cross section of stiffened plate structure

of the stiffener, which represents the thickness of the plate. It is noted that if the ratio of the stiffener length to height is smaller than 10, the beam element cannot be used.

2.2 Mathematical model and iterative formula

To maximize the critical buckling load $\Lambda(\mathbf{A})$, under the given volume constraints, the optimization mathematical model is expressed by (1),

$$
\begin{aligned}
&\text{find} \quad \mathbf{A} = (A_1, A_2, \ldots A_n)^T \\
&\text{max} \quad \Lambda(\mathbf{A}) = \lambda_p = -\frac{\boldsymbol{\varphi}_p^T \mathbf{K} \boldsymbol{\varphi}_p}{\boldsymbol{\varphi}_p^T \mathbf{K}_g \boldsymbol{\varphi}_p} \\
&\text{s.t.} \quad \begin{aligned} &g(A) = v - \eta v_0 \leq 0 \\ &0 < A_{\min} \leq A_i \leq A_{\max} (i = 1, 2, \ldots, n) \end{aligned}
\end{aligned}
\tag{1}
$$

where A_i is the cross-sectional area of the ith stiffener, n is the total number of stiffeners, $g(\mathbf{A})$ is the given volume constraints function, and v and v_0 are the final volume and the initial volume of the whole structure, respectively. η is the volume factor, and $A_{\min}$ and $A_{\max}$ are the lower and upper limits of A_i. In the objective function Λ, λ_p is the pth eigenvalue and $\boldsymbol{\varphi}_p$ is the corresponding eigenvector. $\mathbf{K}$ is the global stiffness matrix, and $\mathbf{K}_g$ is the global geometric stiffness matrix.

The iterative updating formula of the design variable A_i is derived from KKT optimality criterion, as expressed by (2) (Ji et al. 2014):

$$
A_i^{k+1} = \begin{cases} A_{\min} & A_i \leq A_{\min} \\ -\alpha \dfrac{S_i}{\chi l_i} A_i^k + (1-\alpha) A_i^k & A_{\min} < A_i < A_{\max} \\ A_{\max} & A_i \geq A_{\max} \end{cases}
\tag{2}
$$

where k is the iteration number and l_i is the length of the ith stiffener. To ensure convergence, the step factor α is introduced (Chen 1989). The sensitivity S_i of the critical buckling load $\Lambda(\mathbf{A})$ and Lagrange multiplier χ is expressed by (3) and (4), respectively:

$$
S_i = \frac{\partial \Lambda}{\partial A_i}
\tag{3}
$$

$$
\begin{aligned}
\chi &= -\frac{S_i}{A_i^{k+1} l_i} A_i^k = -\frac{A_i^k S_i}{v_i^{k+1}} = -\frac{A_1^k S_1}{v_1^{k+1}} = -\frac{A_2^k S_2}{v_2^{k+1}} = \cdots = -\frac{A_n^k S_n}{v_n^{k+1}} \\
&= -\frac{\sum_{i=1}^{n} A_i^k S_i}{\sum_{i=1}^{n} v_i^{k+1}} = -\frac{\sum_{i=1}^{n} A_i^k S_i}{\eta v_0}
\end{aligned}
\tag{4}
$$

2.3 Sensitivity analysis

The linear buckling behavior of the stiffened plate and shell structure is governed by the generalized eigenvalue problem,

$$
(\mathbf{K} + \lambda_p \mathbf{K}_g) \boldsymbol{\varphi}_p = \mathbf{0}
\tag{5}
$$

If (5) has distinct eigenvalues, the derivative of the eigenvalues λ_p with respect to the design variable A_i is given as (6),

$$
\frac{\partial \lambda_p}{\partial A_i} = -\frac{\boldsymbol{\varphi}_p^T \left[\dfrac{\partial \mathbf{K}}{\partial A_i} + \lambda_p \dfrac{\partial \mathbf{K}_g}{\partial A_i} \right] \boldsymbol{\varphi}_p}{\boldsymbol{\varphi}_p^T \mathbf{K}_g \boldsymbol{\varphi}_p}
\tag{6}
$$

Considering the small change of the cross-sectional area of the ith stiffener A_i, (6) is approximated as the discrete form of (7) in the optimization process,

$$
\Delta \lambda_p = -\frac{\boldsymbol{\varphi}_p^T \left[\Delta \mathbf{K} + \lambda_p \Delta \mathbf{K}_g \right] \boldsymbol{\varphi}_p}{\boldsymbol{\varphi}_p^T \mathbf{K}_g \boldsymbol{\varphi}_p}
\tag{7}
$$

In (7), the change of the global stiffness matrix $\Delta \mathbf{K}$ is equal to the change of the ith stiffener stiffness matrix, which can be obtained. However, $\mathbf{K}_g$ depends on the current stress distribution in the structure, because the cross-sectional area change of the ith stiffener affects the buckling stress in its surrounding stiffeners, and $\mathbf{K}_g$ is not equal to the change of the geometric stiffness matrix of the ith stiffener only. The calculation of $\mathbf{K}_g$ is generally much involved. Nevertheless, for the statically indeterminate structure, $\Delta \mathbf{K}_g$ can be neglected if the cross-sectional area modification at each iteration step is kept sufficiently small, which does not cause a significant change of stress distribution in other stiffeners. By doing so, the change in the pth eigenvalue of the ith stiffener $\Delta \lambda_{ip}$ is given by (8),

$$
\Delta \lambda_{ip} = -\frac{\boldsymbol{\varphi}_{ip}^T \Delta \mathbf{K}_i \boldsymbol{\varphi}_{ip}}{\boldsymbol{\varphi}_p^T \mathbf{K}_g \boldsymbol{\varphi}_p}
\tag{8}
$$

where $\boldsymbol{\varphi}_{ip}$ is the pth eigenvector of the ith stiffener and $\mathbf{K}_i$ is the stiffness matrix of the ith stiffener.

To normalize the eigenvectors in the denominator such that $\boldsymbol{\varphi}_p^T \mathbf{K}_g \boldsymbol{\varphi}_p = 1$, (8) is further rewritten to (9),

$$
\Delta \lambda_{ip} = -\boldsymbol{\varphi}_{ip}^T \Delta \mathbf{K}_i \boldsymbol{\varphi}_{ip}
\tag{9}
$$

where,

$$
\Delta \mathbf{K}_i = \mathbf{K}_i(A_i + \Delta A_i) - \mathbf{K}_i(A_i)
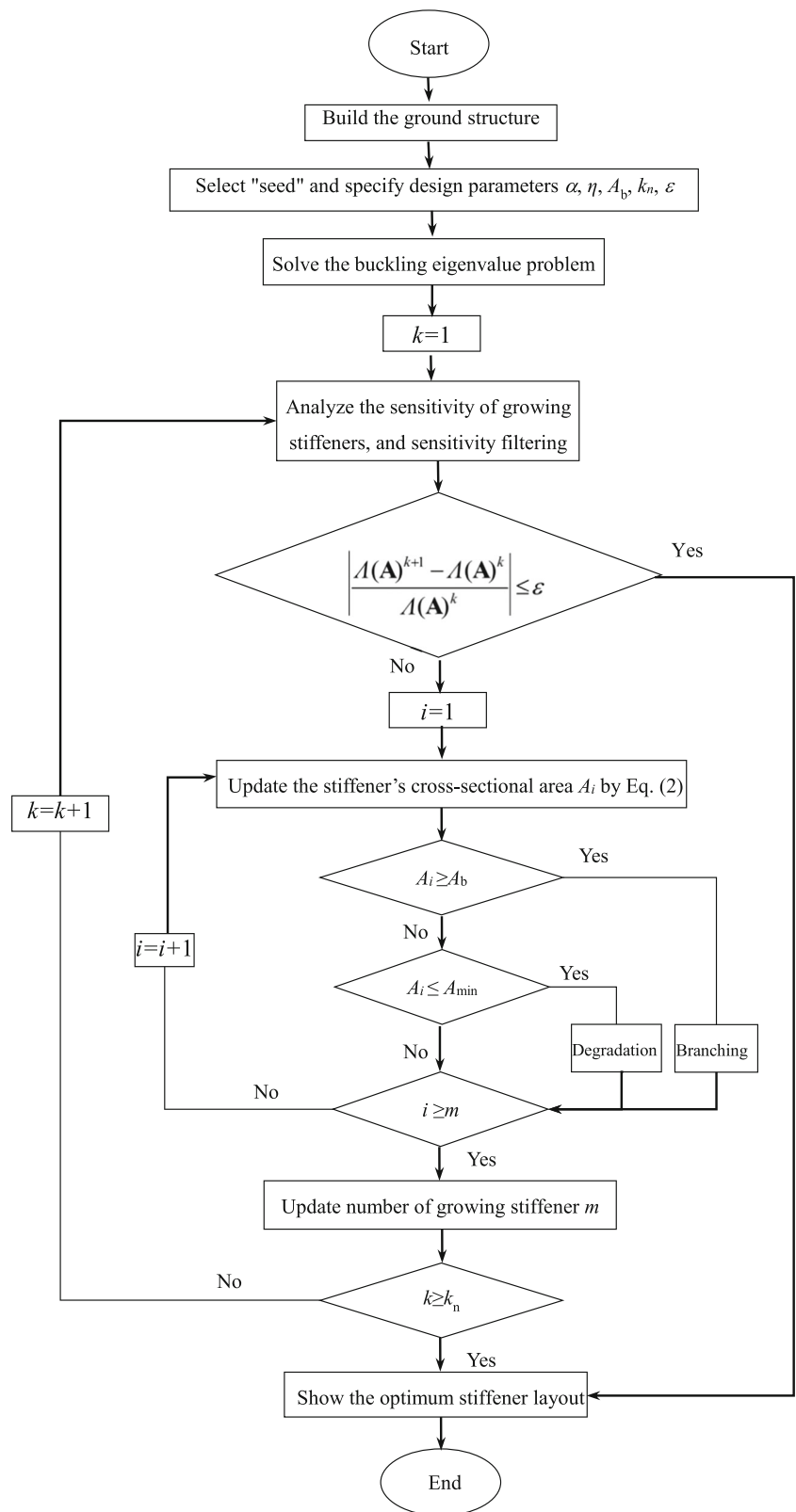\tag{10}
$$

where ΔA_i is the change of the cross-sectional area A_i of the ith stiffener.

Considering λ_p is the design objective $\Lambda(\mathbf{A})$ in (1), the sensitivity S_i in (3) is equal to $\Delta \lambda_{ip}$, that is,

$$
S_i = -\boldsymbol{\varphi}_{ip}^T \Delta \mathbf{K}_i \boldsymbol{\varphi}_{ip}
\tag{11}
$$

It should be noted that (11) is valid only if the distinct eigenvalues exist. However, while the first eigenvalue increases, the subsequent eigenvalues may reduce, and gradually, as the first two or more eigenvalues become very close, it will cause serious interference among themselves. In addition, repeated eigenvalues may occur in physical symmetrically

Fig. 3 Design flowchart of stiffener layout for plate and shell structures

```
                          ┌─────────┐
                          │  Start  │
                          └─────────┘
                               │
                 ┌─────────────────────────────┐
                 │   Build the ground structure │
                 └─────────────────────────────┘
                               │
        ┌──────────────────────────────────────────────────┐
        │ Select "seed" and specify design parameters α, η, A_b, k_n, ε │
        └──────────────────────────────────────────────────┘
                               │
              ┌────────────────────────────────┐
              │ Solve the buckling eigenvalue problem │
              └────────────────────────────────┘
                               │
                          ┌─────────┐
                          │  k=1    │
                          └─────────┘
```

Start

Build the ground structure

Select "seed" and specify design parameters α, η, A_b, k_n, ε

Solve the buckling eigenvalue problem

$k=1$

Analyze the sensitivity of growing stiffeners, and sensitivity filtering

$$\left| \frac{\Lambda(\mathbf{A})^{k+1} - \Lambda(\mathbf{A})^k}{\Lambda(\mathbf{A})^k} \right| \leq \varepsilon \quad \text{Yes}$$

No

$i=1$

Update the stiffener's cross-sectional area A_i by Eq. (2)

$A_i \geq A_b$ Yes

No

$A_i \leq A_{min}$ Yes

No

Degradation   Branching

$i \geq m$ No / Yes

$i=i+1$

Update number of growing stiffener m

$k \geq k_n$ No / Yes

$k=k+1$

Show the optimum stiffener layout

End

stiffened plates due to the quasi-symmetry of the problem. For these cases, multiple eigenvalues are not differentiable in general by (11). In order to deal with existing closely spaced eigenvalues or repeated eigenvalues, an eigenvalue
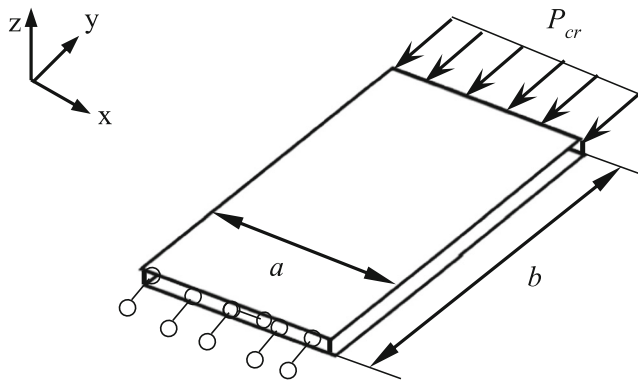
Fig. 4 Design model

$\beta = 5\%$, the sensitivity is taken as the average of S_{i1}, S_{i2}, S_{i3}, ..., S_{iq}, when there are q eigenvalues in the β-neighborhood of λ_1. Consequently, the sensitivity formula is regenerated as shown:

$$S_i = -\frac{1}{q} \sum_{p=1}^{q} \varphi_{ip}^T \Delta K_i \varphi_{ip}$$

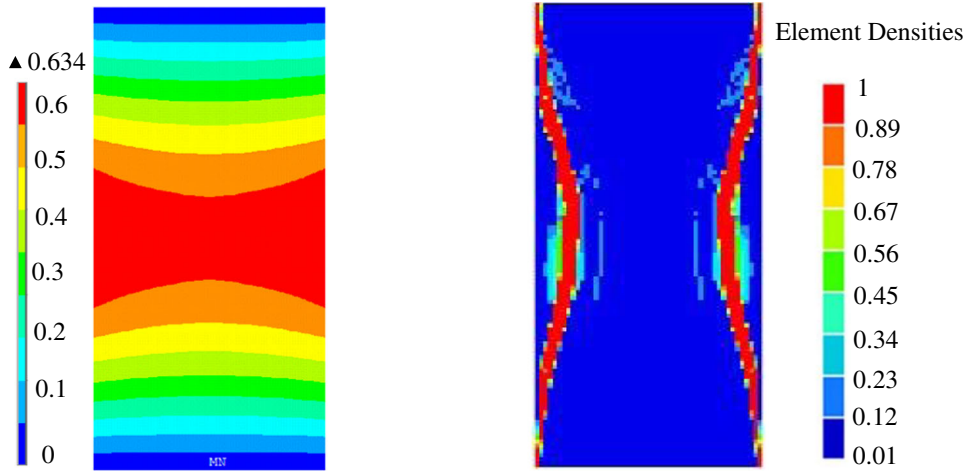$$= -\frac{1}{q} \left(\varphi_{i1}^T \Delta K_i \varphi_{i1} + \varphi_{i2}^T \Delta K_i \varphi_{i2} + \cdots + \varphi_{iq}^T \Delta K_i \varphi_{iq} \right)$$

$$(12)$$

multiplicity parameter β value of $\beta = 5\%$ is introduced (Manickarajah et al. 1998). It means that within the limits of

2.4 Sensitivity filtering

In order to solve the mesh-dependency problem in the process of optimization, the sensitivity filtering scheme that was

Fig. 5 Design result of rectangle plate with simply supported on one edge under unilateral axial pressure. **a** Deformation contour plot of the first buckling mode. **b** Result given by SIMP method. **c** $k = 5$. **d** $k = 200$. **e** $k = 400$

(a) Deformation contour plot of the first buckling mode
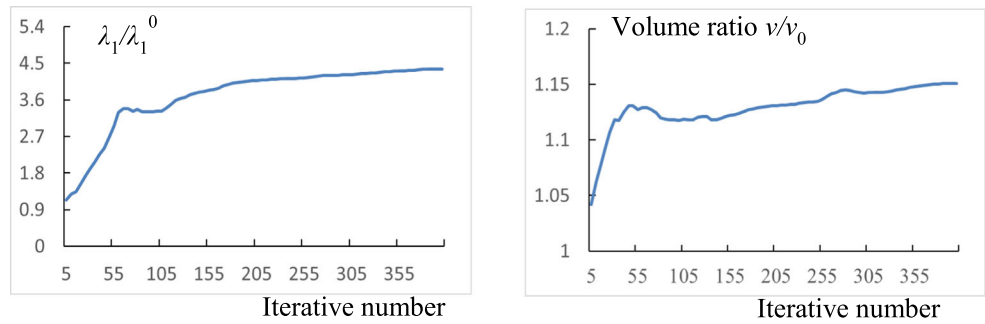

(b) Result given by SIMP method

$\lambda_1/\lambda_1^0 = 1.14 \; v/v_0 = 1.03$

(c) $k=5$

$\lambda_1/\lambda_1^0 = 4 \; v/v_0 = 1.125$

(d) $k=200$

$\lambda_1/\lambda_1^0 = 4.4 \; v/v_0 = 1.15$
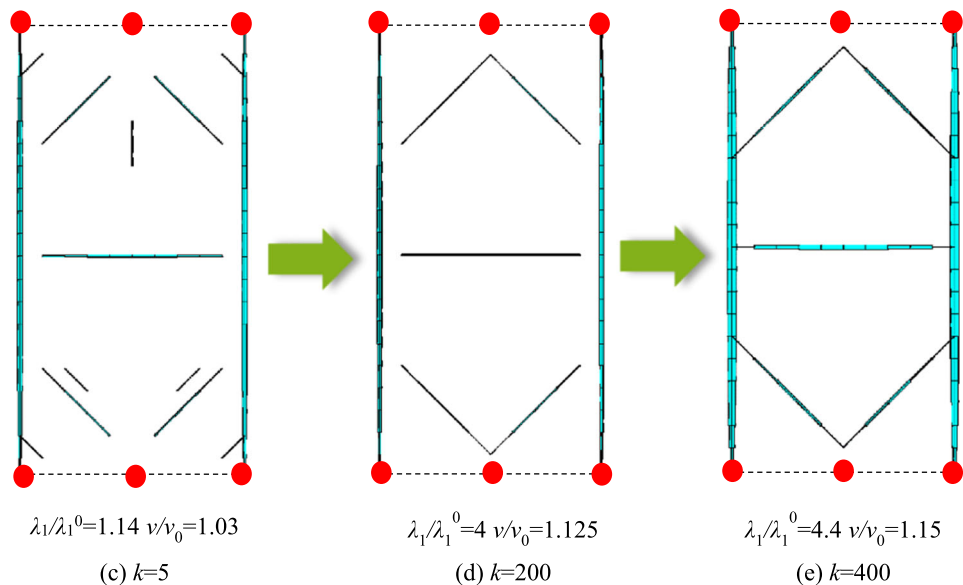
(e) $k=400$

Fig. 6 Iterative history of rectangle plate with simply supported on one edge under unilateral axial pressure. **a** First-order eigenvalue ratio λ_1/λ_1^0. **b** Volume ratio v/v_0

(a) First order eigenvalue ratio λ_1/λ_1^0

(b) Volume ratio v/v_0

Fig. 7 Buckling performance of SIMP design result. **a** Optimized stiffener layout using SIMP method. **b** Deformation contour plot of the first buckling mode under axial pressure $\lambda_1 = 0.715$
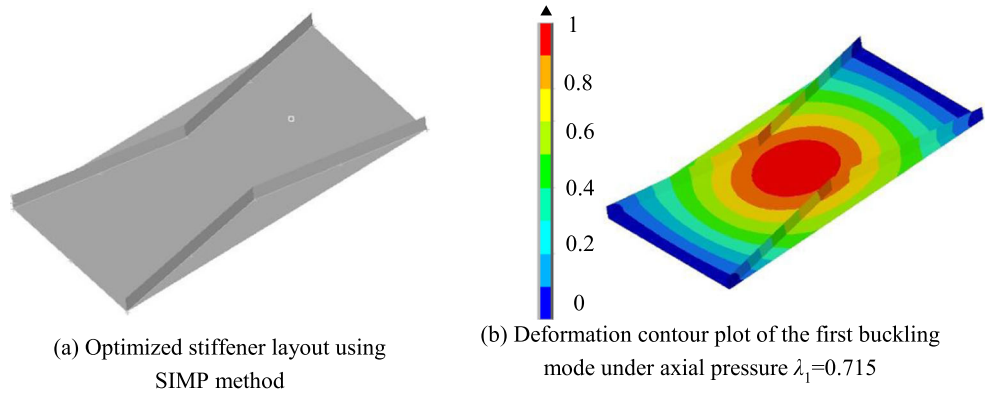
(a) Optimized stiffener layout using SIMP method

(b) Deformation contour plot of the first buckling mode under axial pressure $\lambda_1 = 0.715$

proposed by Sigmund (2007) is adopted. The sensitivity of each stiffener is averaged by its surrounding stiffener sensitivities. The revised sensitivity of the stiffener i is expressed by (13),

$$\overline{S_i} = \frac{1}{A_i \sum\limits_{f=1}^{N} H_f} \sum\limits_{f=1}^{N} H_f A_f S_i \qquad (13)$$

$$H_f = R_{\min} - \text{dist}(i, f) \qquad (14)$$

where S_i is the revised sensitivity, H_f is the weight factor, $R_{\min}$ is the minimum filtering radius, which is equal to 2.5 herein, $\text{dist}(i, f)$ is the distance between the stiffener f located within

the filtering radius and the center of the stiffener i, and N is the total number of stiffeners within the filtering radius.

2.5 Design flowchart

The design flowchart of stiffener layout for plate and shell structures against buckling is shown in Fig. 3. Initially, a ground structure is built, and "seeds" are then selected according to the constraint condition and the loading positions of the structure. Secondly, the iterative step factor α, the initial dimension $A_{\min}$, the branching dimension A_b, and the maximum number of iterations k_n are specified. The convergence

Fig. 8 Buckling performance of AGM design result. **a** Optimized stiffener layout using AGM. **b** Deformation contour plot of the first buckling mode under axial pressure $\lambda_1 = 0.776$
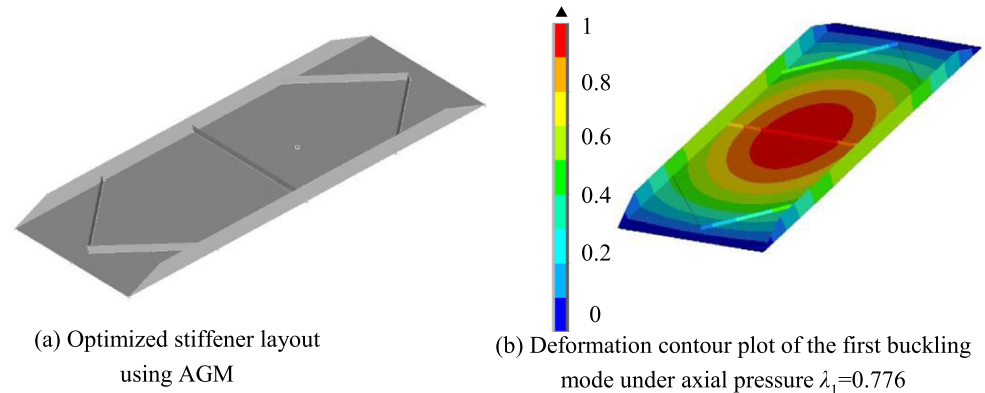
(a) Optimized stiffener layout using AGM

(b) Deformation contour plot of the first buckling mode under axial pressure $\lambda_1 = 0.776$
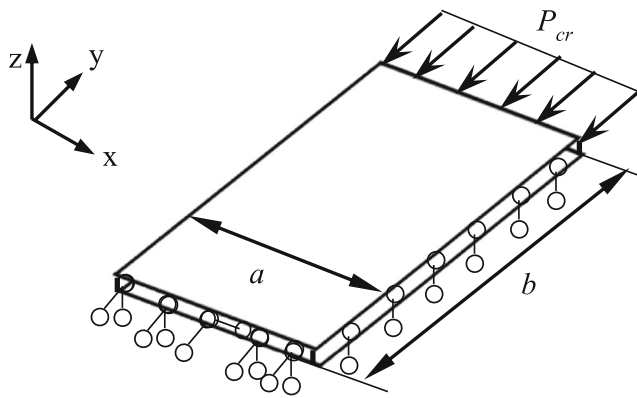
Fig. 9 Design model

tolerance ε is set to be 1×10^{-6} in this study. After that, the kth iteration begins. The structural buckling eigenvalue problem is solved, and the revised sensitivities of the growing stiffeners are evaluated. Next, the design variable A_i is updated according to its sensitivity. If $A_i > A_b$, the stiffener is branched, and all stiffeners around the new branching points are added to the active stiffeners group in the $(k+1)$th iteration. If $A_i < A_{\min}$, the stiffener is degenerated, and it is removed from the active stiffener group in the $(k+1)$th iteration. When all of the active stiffeners in the kth iteration have grown, the number of active stiffeners m is updated, and the iteration continues. If the

difference of the objective value between two successive iterations is smaller than the convergence tolerance ε, or the number of iterations k reaches the maximum value k_n, the iteration process stops. Finally, the optimal stiffener layout is obtained.

3 Design examples

In order to validate the suggested method, several typical examples including imperforated rectangular plates with different aspect ratios and perforated rectangular plates with different holes under pressure or shear loading are studied. In this paper, the Young's modulus is $E = 210$ GPa and the Poisson's ratio is $v = 0.3$. The volume's constraint factor η is set to be 1.15, and the iterative step factor α is 0.05.

3.1 Rectangle plate simply supported on one edge under unilateral axial pressure

Figure 4 shows a rectangle plate supported on one edge under unilateral axial pressure P_{cr}. The width-length ratio of the plate is $a:b = 1:2$. The plate is discretized into 20×10 shell elements and has $20 \times 10 \times 6$ beam elements. Based on the growth principle of AGM, the "seeds" are selected on the

(a) Deformation contour plot of the first buckling mode

(b) Stiffener layout
$\lambda_1/\lambda_1^0 = 1.71$ $v/v_0 = 1.15$
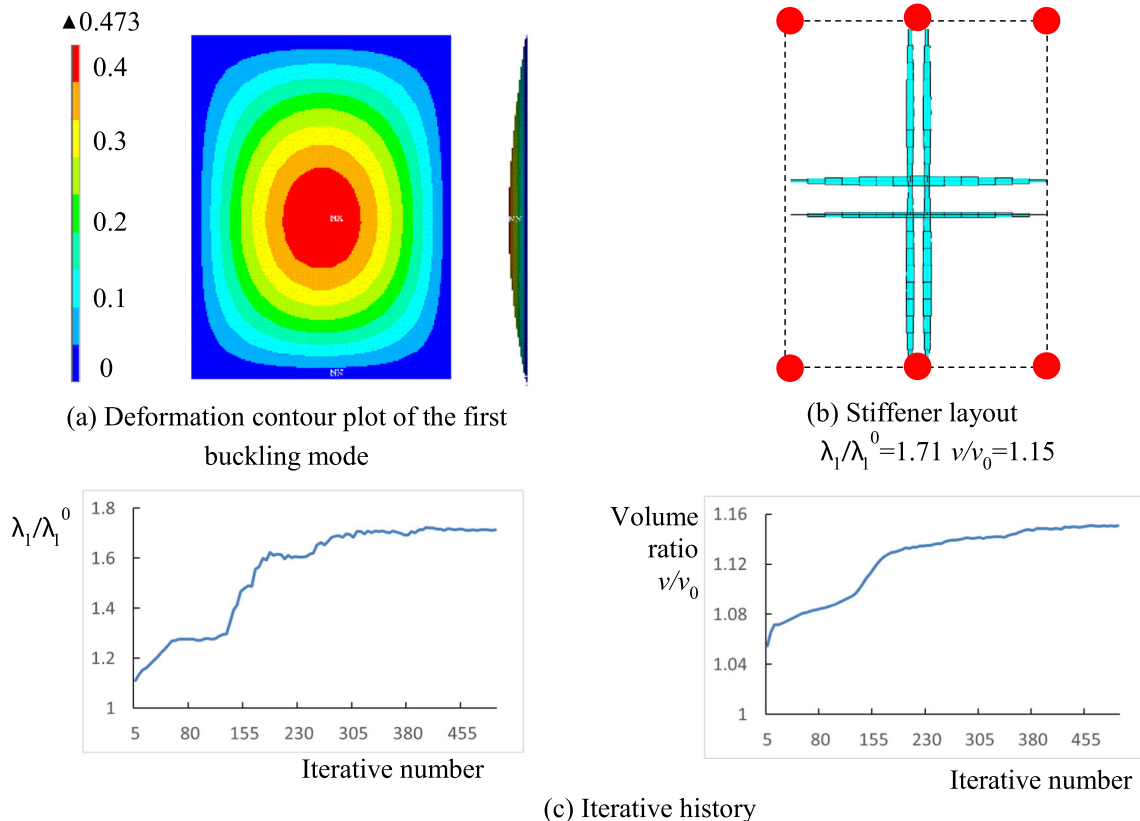

(c) Iterative history

Fig. 10 Design result of the rectangle plate with aspect ratios of 4:3 under unilateral axial pressure. **a** Deformation contour plot of the first buckling mode. **b** Stiffener layout $\lambda_1/\lambda_1^0 = 1.71$ $v/v_0 = 1.15$. **c** Iterative history

supporting and loading edges and are marked with red points shown in Fig. 5. The deformation contour of the first buckling mode is shown in Fig. 5a. Figure 5c–e show the growth process of the stiffeners on the plate when the iteration number k is 5, 200, and 400, respectively. It can be found that the stiffeners grow from the "seeds" and finally connect the loading points and the constraint edges and either grow or degenerate in the growth process. The final layout of the stiffeners is shown in Fig. 5e. From Fig. 5c and e, it is found that two broader vertical stiffeners are formed on both edges of the plate to resist the pressure. Because the deformation in the middle part of the plate is the greatest, the cross sections of the vertical stiffeners in the middle part are relatively larger, and a horizontal stiffener appears at this location. Moreover, two symmetric diagonal stiffeners are formed both in the upper and lower parts. The first-order eigenvalue ratio of the final and the initial plates λ_1/λ_1^0 is 4.4 when the total volume increases by 15%.

Figure 6a shows the iterative history of the first-order eigenvalue ratio λ_1/λ_1^0 and Fig. 6b shows the volume ratio v/v_0. The first-order eigenvalue and the volume increase sharply initially. Due to the continuous growth and degradation of the stiffeners, the stiffener layout does not change greatly, the increase of the first-order eigenvalue changes gradually, and finally remains unchanged. When the structural volume achieves the specified upper limited value, which is $v/v_0 = 1.15$, the stiffener growth stops.

To verify the rationality and effectiveness of the produced stiffener distribution, design results obtained by the SIMP method are shown in Fig. 5b. It is found that the stiffeners are comparatively difficult to identify from the density distribution, and the layout is different from that resulted from AGM. In order to further verify the superiority of the produced stiffener distribution by AGM, a comparative analysis is conducted. Figure 7a shows the stiffened plate based on the SIMP result (Fig. 5b). Figure 7b shows deformation contour plot of the first buckling mode under unilateral axial pressure, and the first-order eigenvalue is $\lambda_1 = 0.715$. Figure 8a shows a stiffened plate based on the AGM result (Fig. 5e). Figure 8b shows deformation contour plot of the first buckling mode under axial pressure and the first-order eigenvalue $\lambda_1 = 0.776$. The first-order eigenvalue λ_1 of the AGM design result increases by 8.5% when compared with the SIMP design result under the same structural volume.

(a) Deformation contour plot of the first buckling mode

(b) Stiffener layout
$\lambda_1/\lambda_1^0 = 2.84$ $v/v_0 = 1.15$
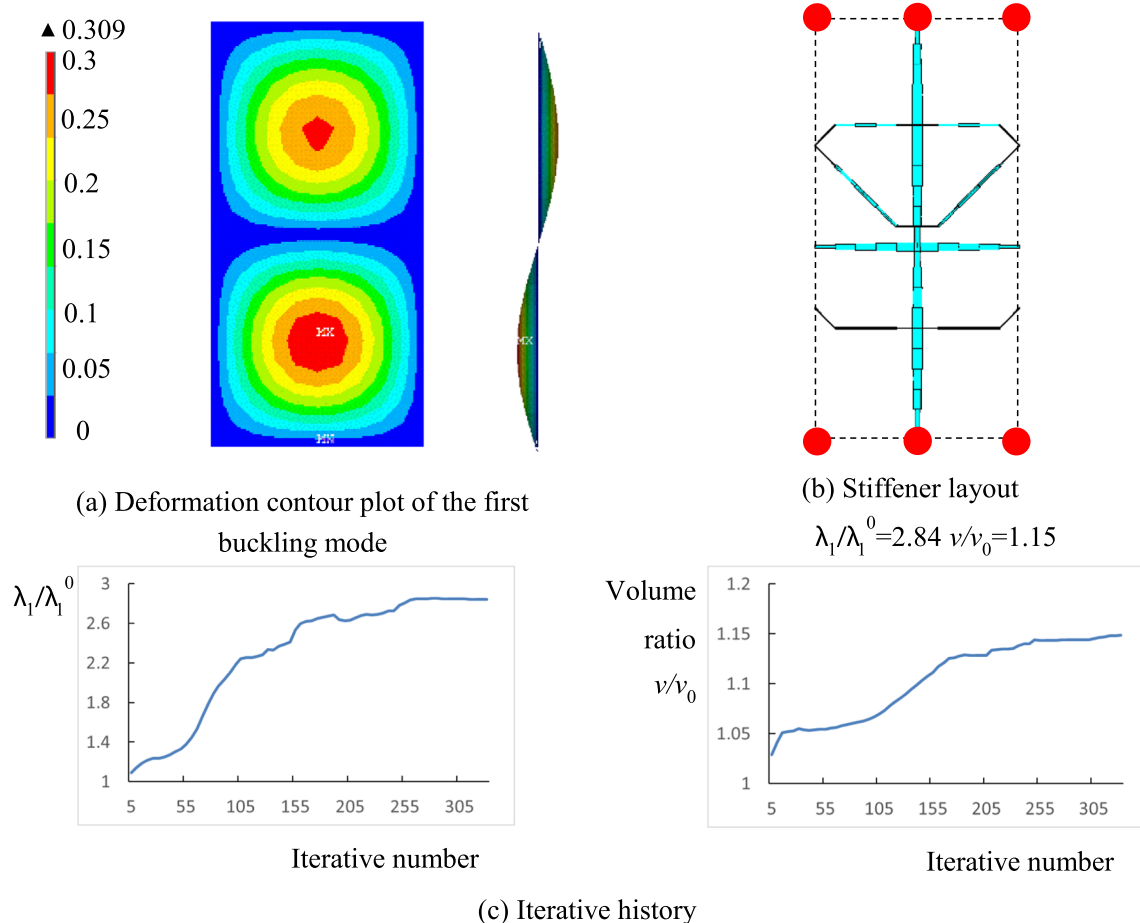
(c) Iterative history

Fig. 11 Design result of the rectangle plate with aspect ratios of 2:1 under unilateral axial pressure. **a** Deformation contour plot of the first buckling mode. **b** Stiffener layout $\lambda_1/\lambda_1^0 = 2.84$ $v/v_0 = 1.15$. **c** Iterative history
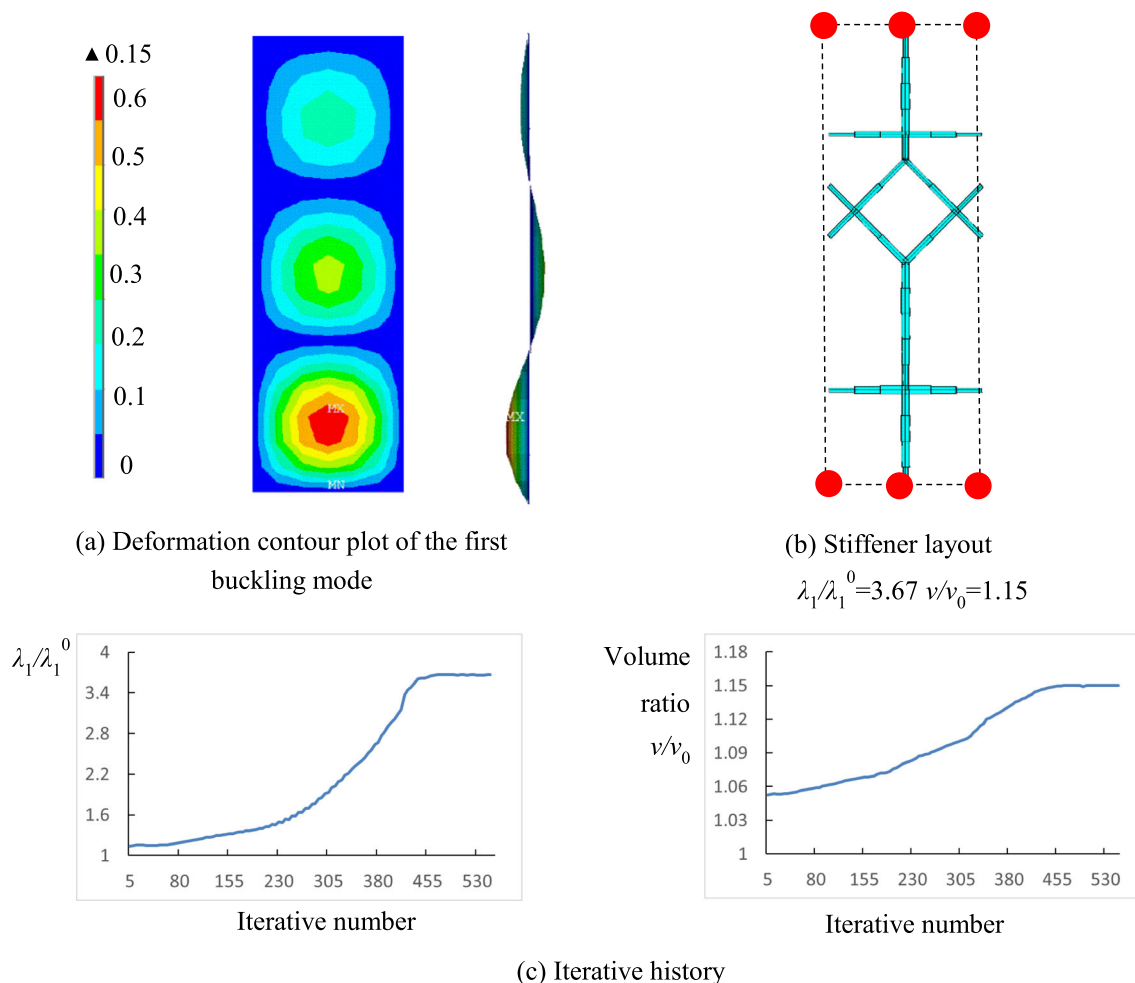
(a) Deformation contour plot of the first
buckling mode

(b) Stiffener layout
λ_1/λ_1^0=3.67 v/v_0=1.15

(c) Iterative history

Fig. 12 Design result of the n rectangle plate with aspect ratios of 3:1 under unilateral axial pressure. **a** Deformation contour plot of the first buckling mode. **b** Stiffener layout $\lambda_1/\lambda_1^0 = 3.67$ $v/v_0 = 1.15$. **c** Iterative history

3.2 Rectangle plate supported on four edges under unilateral axial pressure

Figure 9 shows a rectangle plate supported on four edges under unilateral axial pressure P_{cr}. Three rectangular plates with different aspect ratios of 4:3, 2:1, and 3:1 are shown in Figs. 10, 11, and 12, respectively. In Figs. 10, 11, and 12, panel a shows the deformation contour plot of the first buckling mode, where the left image shows the front view, and the right image shows the side view; panel b shows the final layout of the stiffeners and the selected six "seeds"; and panel c shows the iterative history of the first-order eigenvalue ratio λ_1/λ_1^0 and volume ratio v/v_0. It can be observed that as the plate aspect ratio increases, the number of sinusoidal waveforms of the deformation contour plot of the first buckling mode increases, and the location of stiffeners along the horizontal direction changes correspondingly. As shown in Fig. 10, when the aspect ratio is 4:3, double crisscross stiffeners are located in the central part of the plate. When the aspect ratio is increased to 2:1, as shown in Fig. 11, there is not only one

broader crisscross stiffeners in the center of the plate but also a triangle stiffener frame is formed in the upper part of the plate, connecting the first peak and trough. Additionally, a small horizontal stiffener appears in the second peak wave of the deformation contour plot of the first buckling mode, and when the aspect ratio is 3:1, as shown in Fig. 12, there is a broader vertical stiffener in the center of the plate. In this case, because three half-sine waves appear in the deformation contour plot of the first buckling mode, two broader horizontal stiffeners are formed in the upper and lower parts of the structure respectively. Furthermore, between the first trough and the second peak, a frame stiffener appears. The iterative history of each example shows that both the first-order eigenvalue and the volume all rise by increasing the iterative number initially and gradually reach a stable state. When the structural volume achieves the specified upper limited value, which is $v/v_0 = 1.15$, the optimal layout of the stiffeners is obtained, and the first-order eigenvalue ratio of the final and the initial structure λ_1/λ_1^0 is 1.71, 2.84 and 3.67 respectively.

(a) Rectangle plate with central round-hole

(b) Rectangle plate with central oval-hole

(c) A sample of the FE mesh for a plate
with central round-hole

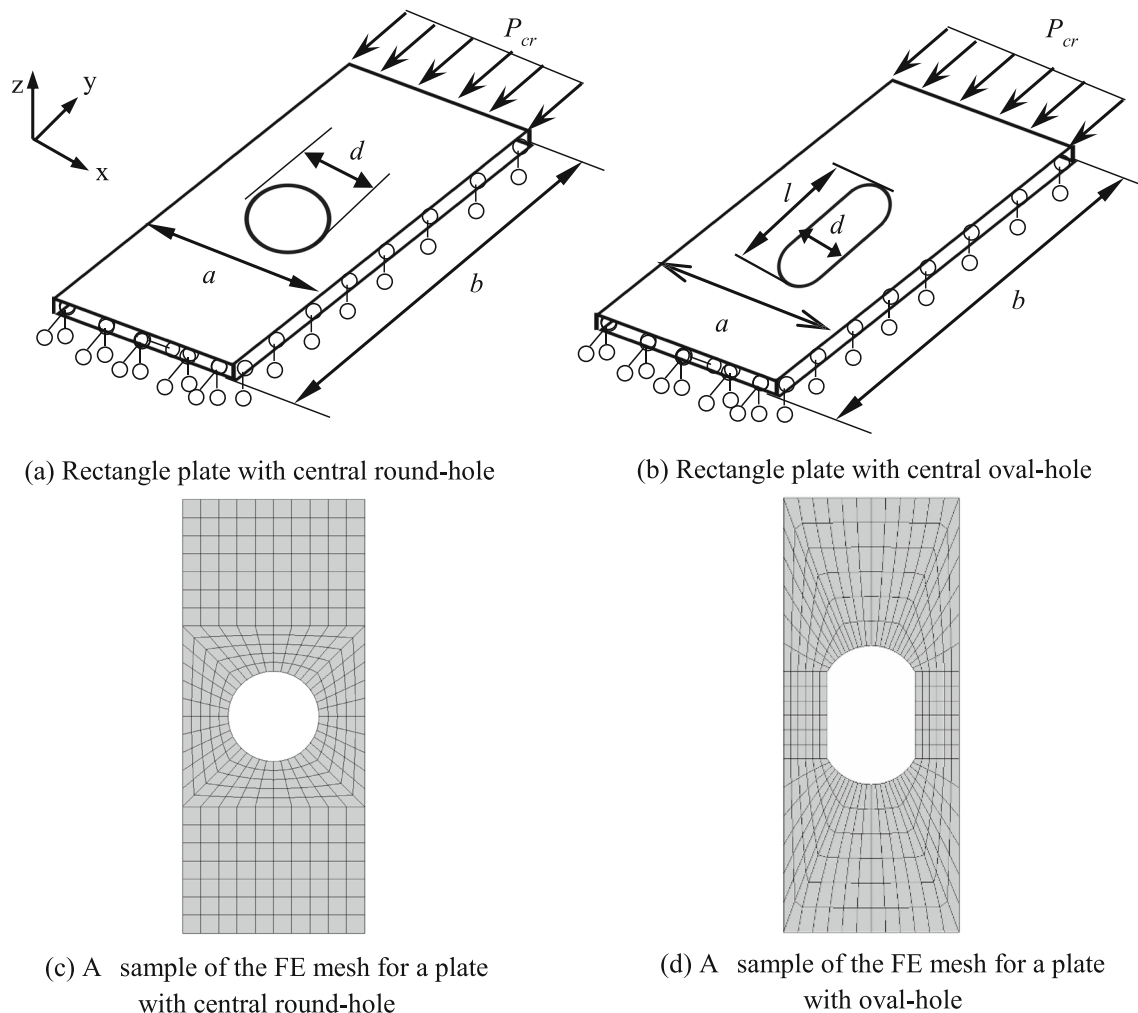(d) A sample of the FE mesh for a plate
with oval-hole

Fig. 13 Design model. **a** Rectangle plate with central round hole. **b** Rectangle plate with central oval hole. **c** A sample of the FE mesh for a plate with central round hole. **d** A sample of the FE mesh for a plate with oval hole

3.3 Perforated rectangle plates simply supported on four edges under unilateral axial pressure

Figure 13 shows two perforated rectangle plates supported on four edges under unilateral axial pressure P_{cr}, in which one has a central round hole shown in Fig. 10a, and the other has a central oval hole shown in Fig. 13b. Both the diameter of the round hole and the minor axis of the ellipse are d, and the major axis of the ellipse is l. The geometric ratios of the plate shown in Fig. 10 are $a{:}b = 1{:}2.4$, $d{:}a = 1{:}2$, and $l{:}b = 1{:}3$. Figure 13c and d are the FE mesh for the plates with a central round hole and an oval hole respectively. These two plates are discretized into 340 and 360 shell elements and have 340×6 and 360×6 beam elements respectively.

Figures 14 and 15 show the design results, where the figure arrangements are replicated from Fig. 12. By comparing Fig. 14b with Fig. 15b, it is found that the stiffeners grow to adapt to the different shape of the hole although the final layout of the stiffeners is similar. It is found that there is a

broader vertical stiffener in the center of each plate to directly bear the axial pressure, and in the center of each plate where the deformation is maximum, there are two crisscross stiffeners connecting to the stiffeners around the hole to resist the deformation. When the structural volume reaches 1.15 times of the initial volume, the first-order eigenvalue ratios of the final and the initial plates λ_1/λ_1^0 are 2.7 and 3.86 respectively.

From an engineering perspective, perforated steel plates are widely used in the aerospace and ship industry. To enhance mechanical performance, placing stiffeners on perforated plates is a preferred option. Figure 16a shows a stiffened perforated steel plate, which is widely used in ship structures. The dimensions of the plate are 1000 mm × 2400 mm × 20 mm, the diameter of the central cutout is 500 mm, and the height of the stiffener is 100 mm. Figure 16b shows a deformation contour plot of the first buckling mode under unilateral axial pressure, and the first-order eigenvalue is $\lambda_1 = 0.429$. Figure 17a shows the optimized stiffened perforated plates
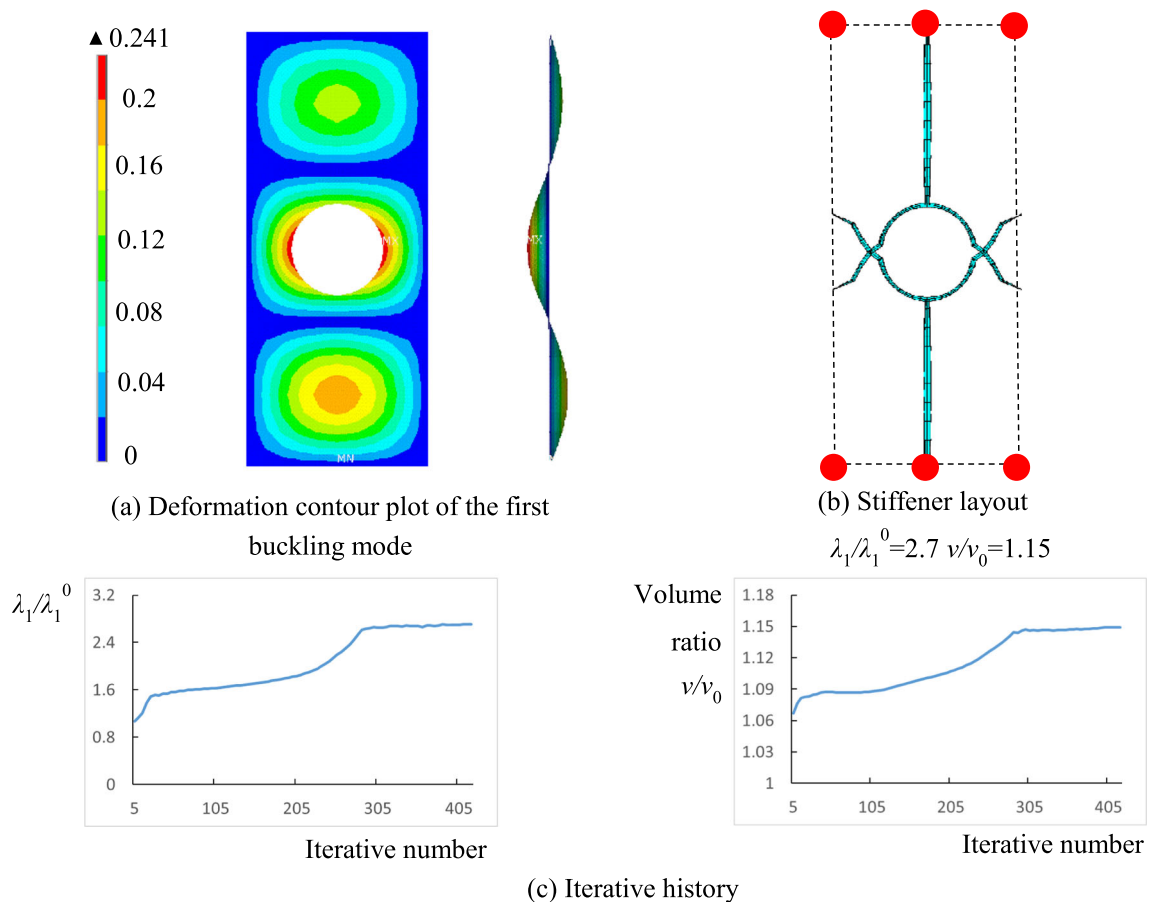
(a) Deformation contour plot of the first
buckling mode

(b) Stiffener layout
$\lambda_1/\lambda_1^0 = 2.7 \, v/v_0 = 1.15$

(c) Iterative history

Fig. 14 Design result of rectangle plate with central round-hole under unilateral axial pressure. **a** Deformation contour plot of the first buckling mode. **b** Stiffener layout $\lambda_1/\lambda_1^0 = 2.7 \, v/v_0 = 1.15$. **c** Iterative history

according to Fig. 14b. The volumes of the two structures shown in Figs. 16a and 17a are equivalent. Figure 17b shows the deformation contour plot of the first buckling mode under axial pressure, where the first-order eigenvalue is $\lambda_1 = 0.496$. It can be concluded that the first-order eigenvalue λ_1 of the optimized stiffener layout increases by 15.6% by comparing with the empirical design.

a stable state. When the structural volume reaches 1.15 times the initial volume, the ratio of the ultimate first-order eigenvalue ratio λ_1/λ_1^0 is 6.27. Figure 19c shows the density distribution patterns given by the SIMP method. It is found that the density distribution shows a certain similarity with that resulted from AGM, but it is difficult to obtain the real stiffener layout.

3.4 Square plate with simply supported on four edges under shear loading

Figure 18 shows a shear loading square plate supported on four edges. Figure 19a shows the deformation contour plot of the first buckling mode. The maximum deformation occurs along the diagonal direction; therefore, five parallel diagonal stiffeners are formed perpendicular to the deformation direction to resist the shear load, as shown in Fig. 19b. Figure 19d shows the iterative history of the first-order eigenvalue ratio λ_1/λ_1^0 and volume ratio v/v_0, respectively. It is also found that as the iteration number increases, the first-order eigenvalue and its corresponding volume both increase and finally reach

3.5 Perforated rectangle plates simply supported on four edges under shear loading

Figure 20 shows two rectangle plates supported on four edges under shear loading τ_{cr}, in which one has a central round-hole shown in Fig. 20a, and another has a central oval-hole shown in Fig. 20b. The other parameters are as same as Sect. 3.3.

Figures 21 and 22 show the design results. Four "seeds" are selected at the corners of the plates. As shown in Fig. 21b, there are several parallel broader diagonal stiffeners, which have a similar appearance to Fig. 19b, but with curved ripple-like stiffeners near the hole. However, in the case of the oval-hole, as shown in Fig. 20b, the stiffener layout is very
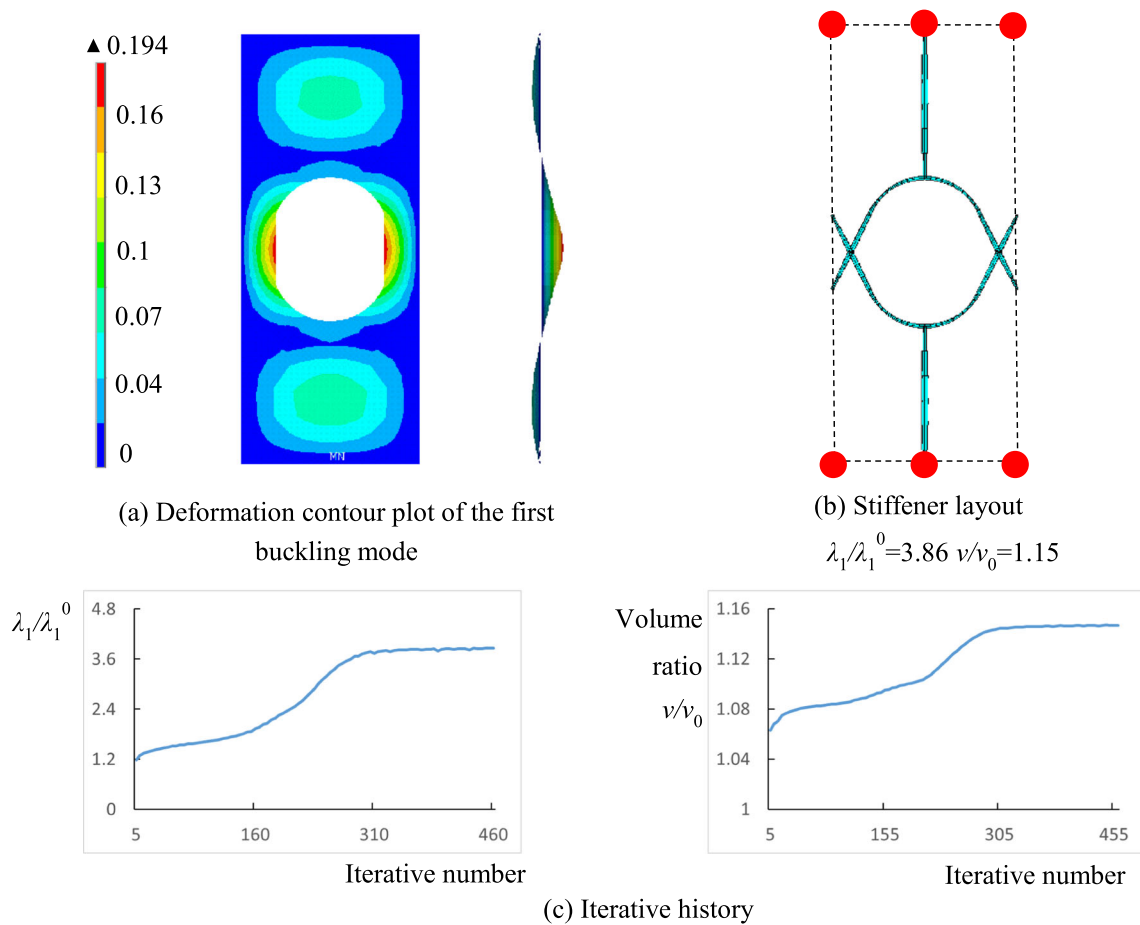
(a) Deformation contour plot of the first buckling mode

(b) Stiffener layout
$\lambda_1/\lambda_1^0 = 3.86$ $v/v_0 = 1.15$

(c) Iterative history

Fig. 15 Design result of the rectangle plate with central oval-hole under unilateral axial pressure. **a** Deformation contour plot of the first buckling mode. **b** Stiffener layout $\lambda_1/\lambda_1^0 = 3.68$ $v/v_0 = 1.15$. **c** Iterative history

different from Figs. 19b and 22b. The oval hole almost destroys the parallel diagonal stiffener layout; instead, petal-like stiffeners formed by small stiffeners reinforce the main diagonal stiffener. The first-order eigenvalue ratio of the final and the initial plates λ_1/λ_1^0 is 4.85 and 8.88, respectively. Figures 21c and 22c show the density distribution patterns given by the SIMP method. It also can be found that the density distributions are similar with that resulted from AGM, but because the density distributions do not continue, the real stiffener layouts cannot be obtained directly.

4 Conclusions

AGM is applied to design the stiffener layout for enhancing the buckling resistance of plate and shell structures. Inspired

Fig. 16 Buckling performance of empirical design. **a** Original stiffener layout. **b** Deformation contour plot of the first buckling mode under axial pressure $\lambda_1 = 0.429$
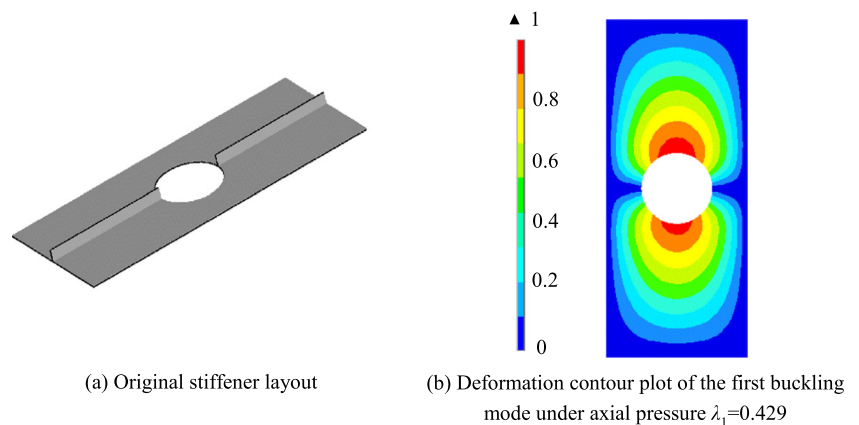

(a) Original stiffener layout

(b) Deformation contour plot of the first buckling mode under axial pressure $\lambda_1 = 0.429$

Fig. 17 Buckling performance of optimal design. **a** Original stiffener layout. **b** Deformation contour plot of the first buckling mode under axial pressure $\lambda_1 = 0.576$
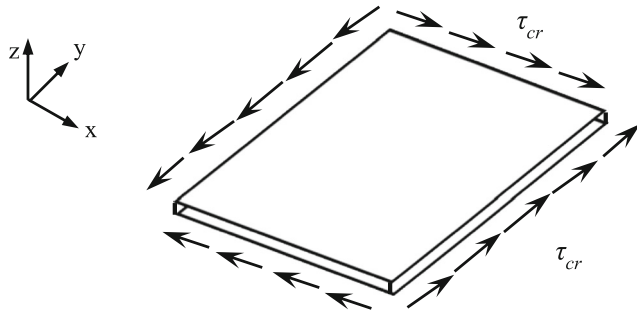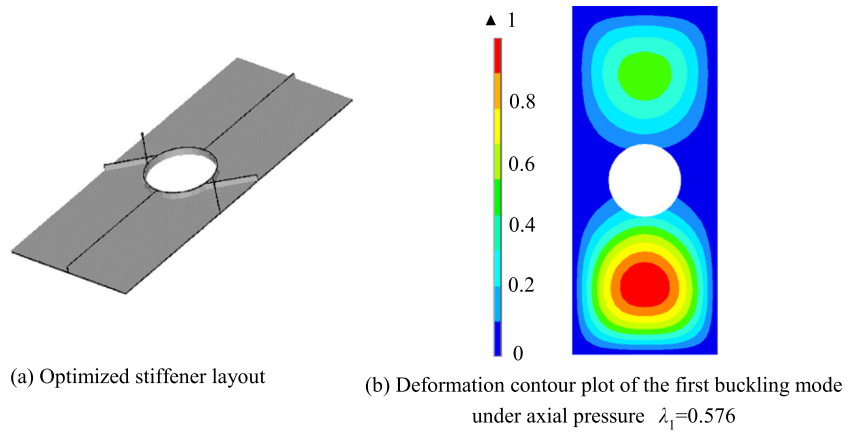

(a) Optimized stiffener layout

(b) Deformation contour plot of the first buckling mode under axial pressure $\lambda_1 = 0.576$

Fig. 18 Design model

by the bionic growth principle, clear and continuous stiffener layout can be obtained, and the buckling performance of the optimized structures is greatly enhanced.

Considering the practical application of stiffened plate and shell structures, especially for aerospace and ship structures, several typical design examples, including imperforated and perforated rectangular plates with unilateral axial pressure and shear loading, are studied. Unlike general stiffener layouts, distinctive stiffener layouts are obtained, which reveal the following design principles of

(a) Deformation contour plot of the first buckling mode

(b) Stiffener layout $\lambda_1/\lambda_1^0 = 6.27$ $v/v_0 = 1.15$

(c) Result given by SIMP method
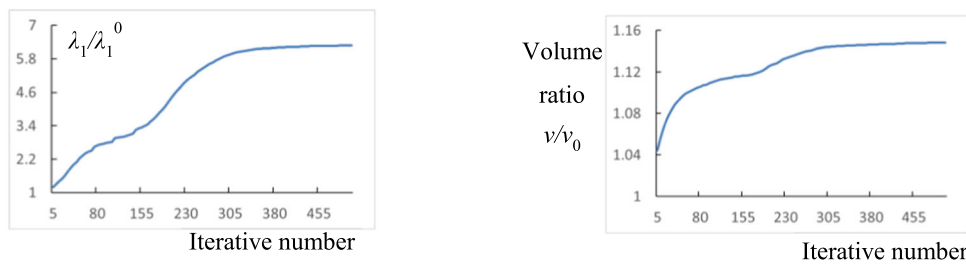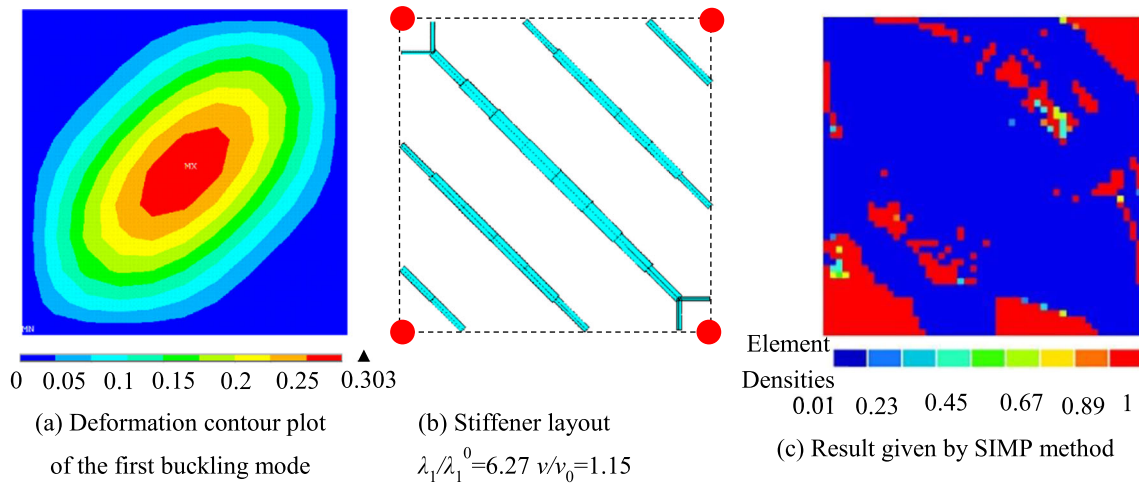
(d) Iterative history

Fig. 19 Design results of the square plate with simply supported on four edges under shear loading. **a** Deformation contour plot of the first buckling mode. **b** Stiffener layout $\lambda_1/\lambda_1^0 = 6.27$ $v/v_0 = 1.15$. **c** Result given by SIMP method. **d** Iterative history

Fig. 20 Design model. **a** Rectangle plate with central round hole. **b** Rectangle plate with central oval hole

(a) Rectangle plate with central round-hole

(b) Rectangle plate with central oval-hole
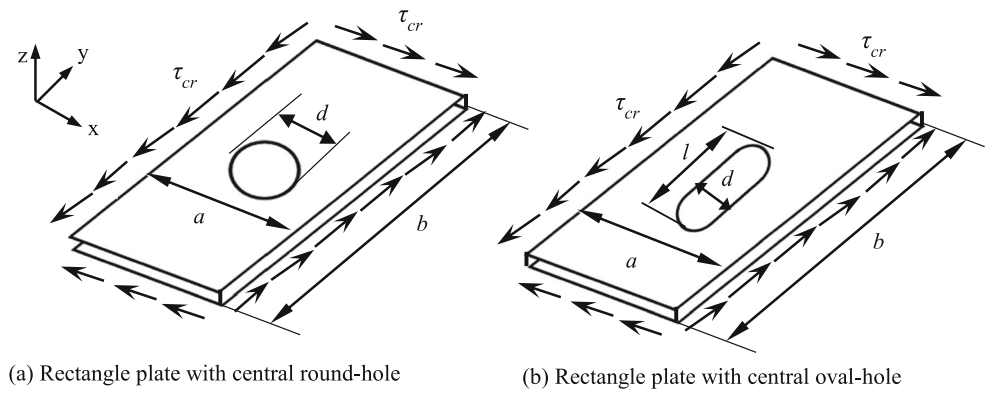
stiffened plate and shell structures to resist buckling. (1) Under unilateral axial pressure, a broader vertical stiffener in the central part of structure is crucial, which resists directly the pressure load. As the plate aspect ratios increases, some horizontal stiffeners distribute in the peak or trough of the deformation of the first buckling mode, and frame stiffeners connecting the peak and trough further strengthen the structures against buckling. (2) Under shear loading, due to the maximum deformation taking place along the diagonal direction, parallel diagonal stiffeners are formed perpendicular to the deformation direction to resist the shear load. (3) In the case of perforated plate structures, stiffeners grow adapting to the different shape of the hole, and form curved ripple-like or petal-like

(a) Deformation contour plot of the first buckling mode

(b) Stiffener layout $\lambda_1/\lambda_1^0 = 4.85$ $v/v_0 = 1.15$

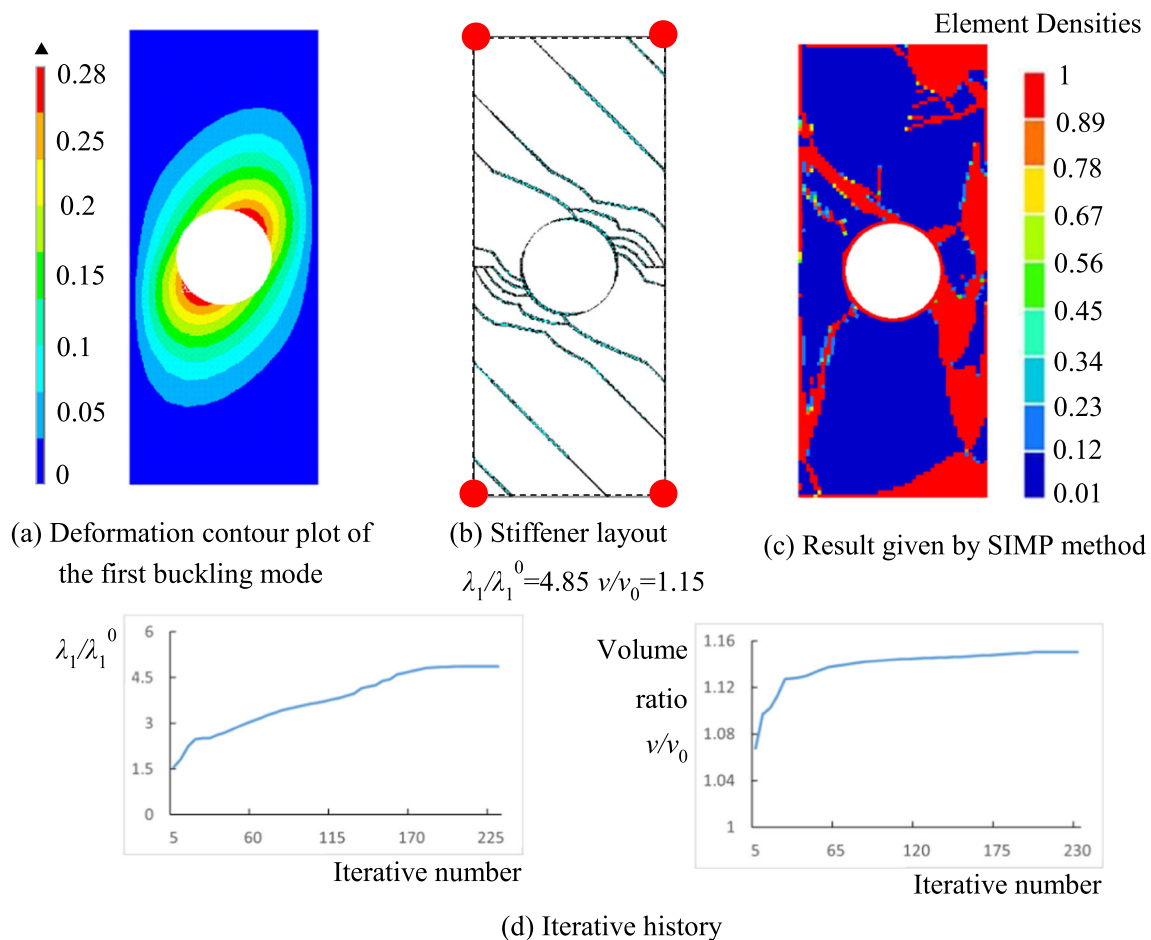(c) Result given by SIMP method

(d) Iterative history

Fig. 21 Design result of the rectangle plate with central round-hole under shear loading. **a** Deformation contour plot of the first buckling mode. **b** Stiffener layout $\lambda_1/\lambda_1^0 = 4.85$ $v/v_0 = 1.15$. **c** Result given by SIMP method. **d** Iterative history

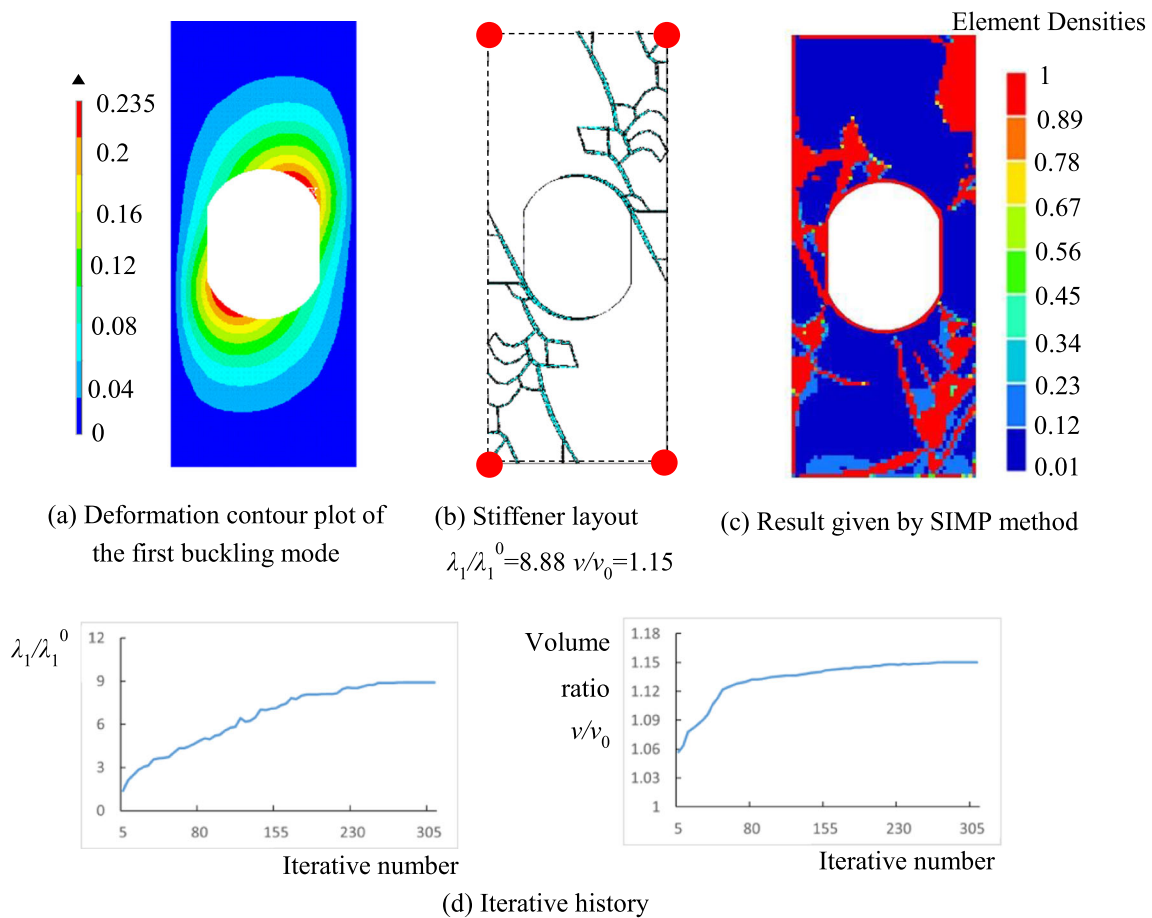(a) Deformation contour plot of the first buckling mode

(b) Stiffener layout λ_1/λ_1^0=8.88 v/v_0=1.15

(c) Result given by SIMP method

(d) Iterative history

Fig. 22 Design result of the rectangle plate with central oval-hole under shear loading. **a** Deformation contour plot of the first buckling mode. **b** Stiffener layout $\lambda_1/\lambda_1^0 = 8.88$ $v/v_0 = 1.15$. **c** Result given by SIMP method. **d** Iterative history

special stiffener layouts. The design results show that AGM is effective to deal with the buckling problem, and it is expected that AGM can be applied to more complex practical engineering structures and the revealed design principles may guide engineers to design more effective stiffened plate and shell structures to resist buckling. (4) Because of the bionic growth mechanism, AGM is more efficient to achieve a clearer design result that includes concise distribution of the stiffeners compared with the traditional topology design method.

5 Replication of results

AGM iterative process is written by APDL (ANSYS), combining with the structural analysis by ANSYS. The iterative process includes the following parts.

Part 1: Ground structure construction

```
*do,j,1,nshell,1
*if,elem_node(3,j),eq,elem_node(4,j),then
nsel,s,node,,elem_node(1,j)
nsel,a,node,,elem_node(2,j)
```

```
esln,s,1,active
*if,elmiqr(0,13),eq,0,then
k=k+1
nsec=nsec+1 nloc_x=(nx(elem_node(1,j))+
nx(elem_node(2,j)))/2+
normnx(elem_node(1,j),elem_node(2,j),elem_node(3,j))*dis-
tnd(elem_node(1,j),elem_node(2,j))
nloc_y=(ny(elem_node(1,j))+ny(elem_node(2,j)))/2+
normny(elem_node(1,j),elem_node(2,j),elem_node(3,j))*dis-
tnd(elem_node(1,j),elem_node(2,j))
nloc_z=(nz(elem_node(1,j))+nz(elem_node(2,j)))/2+
normnz(elem_node(1,j),elem_
node(2,j),elem_node(3,j))*distnd(elem_node(1,j),
elem_node(2,j))
   n,k,nloc_x,nloc_y,nloc_z
   sectype,nsec,beam,bst,root
   secdata,width,height
   secoffset,cent
   secnum,nsec
   e,elem_node(1,j),elem_node(2,j),k
*endif
allsel
```

```
*endif
*enddo
```

Part 2: Update process

The design variables update according to (2). The sensitivity is calculated by analytical method, in which the stiffness matrix of beam element is input directly.

Part 3: Degradation and Branching:

```
*get,numet,etyp,,num,max
*vget,r(1,1),elem, nshell +1,node,1,,,2
*vget,r(1,2),elem, nshell +1,node,2,,,2
*vget,r(1,3),elem, nshell +1,node,3,,,2
*vget,r(1,4),elem, nshell +1,esel,,,,2
*do,j,1,numrib,1
*if,r(j,5),eq, A0,then
r(j,9)=r(j,9)+1
*else
r(j,9)=0
*endif
*enddo
*do,j,1,numrib,1
*if,r(j,9),ge,2,then
r(j,4)=-1
*endif
*enddo
nsel,none
*do,j,1,numrib,1
*if,r(j,5),ge, Ab,and,r(j,4),eq,1,then
nsel,a,node,,r(j,1)
nsel,a,node,,r(j,2)
*endif
*enddo
esel,s,type,,numet+1
esln,r,0,all
*do,j,1,numrib,1
*if,elmiqr(nshelem+j,1),eq,1,then
r(j,4)=1
*endif
*enddo
allsel
```

Compliance with ethical standards

Conflict of interest The authors declare that there is no conflict of interest.

References

Alinia MM (2005) A study into optimization of stiffeners in plates subjected to shear loading. Thin-Walled Struct 43(5):845–860

Alinia MM, Moosavi SH (2009) Stability of longitudinally stiffened web plates under interactive shear and bending forces. Thin-Walled Struct 47(1):53–60

Alinia MM, Hosseinzadeh SAA, Habashi HR (2007) Numerical modelling for buckling analysis of cracked shear panels. Thin-Walled Struct 45(12):1058–1067

Alinia MM, Hosseinzadeh SAA, Habashi HR (2008) Numerical modelling for buckling analysis of cracked shear panels. J Constr Steel Res 64(12):1483–1494

An HC, Chen SY, Huang H (2018) Multi-objective optimization of a composite stiffened panel for hybrid design of stiffener layout and laminate stacking sequence. Struct Multidiscip Optim 57(4):1411–1426

An HC, Chen SY, Huang H (2019) Concurrent optimization of stacking sequence and stiffener layout of a composite stiffened panel. Eng Optim 51(4):608–626

Bendsoe MP, Sigmund O (2003) Topology optimization: theory, methods and applications. Springer, Berlin

Butler R, Lillico M, Hunt GW, McDonald NJ (2001) Experiments on interactive buckling in optimized stiffened panels. Struct Multidiscip Optim 23(1):40–48

Carlos C (2015) Patch loading resistance of longitudinally stiffened girders - a systematic review. Thin-Walled Struct 95:1–6

Cevik A (2007) A new formulation for longitudinally stiffened webs subjected to patch loading. J Constr Steel Res 63(10):1328–1340

Cevik A, Gogus MT, GuzelbeY IH, Filiz H (2010) A new formulation for longitudinally stiffened webs subjected to patch loading using stepwise regression method. Adv Eng Softw 41(4):611–618

Chacon R, Mirambell E, Real E (2013a) Transversally stiffened plate girders subjected to patch loading. Part 1. Preliminary study. J Constr Steel Res 80:483–491

Chacon R, Mirambell E, Real E (2013b) Transversally stiffened plate girders subjected to patch loading. Part 2. Additional numerical study and design proposal. J Constr Steel Res 80:492–504

Chacon R, Mirambell E, Real E (2014) Influence of flange strength on transversally stiffened girders subjected to patch loading. J Constr Steel Res 97:39–47

Chacon R, Herrera J, Fargier-Gabaldon L (2017) Improved design of transversally stiffened steel plate girders subjected to patch loading. Eng Struct 150:774–785

Chen SX (1989) Slack factor iteration for solving non-linear coupled equations. J Harbin Archit Civ Eng INST 21(3):1–11

Chen SY, Dong TS, Shui XF (2019) Simultaneous distribution and sizing optimization for stiffeners with an improved genetic algorithm with two-level approximation. Eng Optim Published online. https://doi.org/10.1080/0305215X.2018.1558444

Cheng GD, Xu L (2016) Two-scale topology design optimization of stiffened or porous plate subject to out-of-plane buckling constraint. Struct Multidiscip Optim 54(5):1283–1296

Ding XH, Yamazaki K (2004) Stiffener layout design for plate structures by growing and branching tree model (application to vibration-proof design). Struct Multidiscip Optim 26(1–2):99–110

Ding XH, Yamazaki K (2005) Adaptive growth technique of stiffener layout pattern for plate and shell structures to achieve minimum compliance. Eng Optim 37(3):259–276

Gao XJ, Ma HT (2015) Topology optimization of continuum structures under buckling constraints. Comput Struct 157:142–152

Hao P, Wang B, Tian K, Li G, Du K, Niu F (2016) Efficient optimization of cylindrical stiffened shells with reinforced cutouts by curvilinear stiffeners. AIAA J 54(4):1350–1363

Hao P, Wang YT, Liu C, Wang B, Tian K, Li G, Wang Q, Jiang LL (2018) Hierarchical nondeterministic optimization of curvilinearly stiffened panel with multicutouts. AIAA J 56(10):4180–4194

Huang H, An HC, Ma HB, Chen SY (2019) An engineering method for complex structural optimization involving both size and topology design variables. Int J Numer Methods Eng 117(3):291–315

Issa-El-Khoury G, Linzell DG, Geschwindner LF (2016) Flexure-shear interaction influence on curved, plate girder web longitudinal stiffener placement. J Constr Steel Res 120:25–32

Ji J, Ding XH, Xiong M (2014) Optimal stiffener layout of plate/shell structures by bionic growth method. Comput Struct 135(135):88–99

Kasaiezadeh A, Khajepour A, Jahed H (2010) Using level set method in order to design structures against buckling. Proceedings of the ASME International Design Engineering Technical Conference, pp 1225–1231

Komur MA, Sonmez M (2015) Elastic buckling behavior of rectangular plates with holes subjected to partial edge loading. J Constr Steel Res 112:54–60

Luo QT, Tong LY (2015) Structural topology optimization for maximum linear buckling loads by using a moving iso-surface threshold method. Struct Multidiscip Optim 52(1):71–90

Maiorana E, Pellegrino C, Modena C (2011) Influence of longitudinal stiffeners on elastic stability of girder webs. J Constr Steel Res 67(1):51–64

Manickarajah D, Xie YM, Steven GP (1995) A simple method for the optimization of columns, frames and plates against buckling. International Conference on Structural Stability and Design, pp 174–180

Manickarajah D, Xie YM, Steven GP (1998) An evolutionary method for optimization of plate buckling resistance. Finite Elem Anal Des 29(3–4):205–230

Mohammadzadeh B, Choi E, Kim WJ (2018) Comprehensive investigation of buckling behavior of plates considering effects of holes. Struct Eng Mech 68(2):261–275

Nelson L, Carlos G, Rolando C, Euro C (2017) Influence of bearing length on the patch loading resistance of multiple longitudinally stiffened webs. EUROSTEEL, Copenhagen, pp 4199–4204

Neves MM, Rodrigues H, Guedes JM (1995) Generalized topology design of structures with a buckling load criterion. Struct Optim 10(2):71–78

Paik JK (2007) Ultimate strength of perforated steel plates under edge shear loading. Thin-Walled Struct 45(3):301–306

Paik JK (2008) Ultimate strength of perforated steel plates under combined blaxial compression and edge shear loads. Thin-Walled Struct 46(2):207–213

Pavlovcic L, Detzel A, Kuhlmann U, Beg D (2007a) Shear resistance of longitudinally stiffened panels - part 1: tests and numerical analysis of imperfections. J Constr Steel Res 63(3):337–350

Pavlovcic L, Beg D, Kuhlmann U (2007b) Shear resistance of longitudinally stiffened panels - part 2: numerical parametric study. J Constr Steel Res 63(3):351–364

Shimoda M, Okada T, Nagano T, Shi JX (2016) Free-form optimization method for buckling of shell structures under out-of-plane and in-plane shape variations. Struct Multidiscip Optim 54(2):275–288

Sigmund O (2007) Morphology-based black and white filters for topology optimization. Struct Multidiscip Optim 33(4–5):401–424

Wang B, Hao P, Li G, Tian K, Du KF, Wang XJ, Zhang X, Tang XH (2014) Two-stage size-layout optimization of axially compressed stiffened panels. Struct Multidiscip Optim 50(2):313–327

Wang D, Abdalla MM, Zhang WH (2017) Buckling optimization design of curved stiffeners for grid-stiffened composite structures. Compos Struct 159:656–666

Wang D, Abdalla MM, Wang ZP, Su ZC (2019) Streamline stiffener path optimization (SSPO) for embedded stiffener layout design of non-uniform curved grid-stiffened composite (NCGC) structures. Comput Methods Appl Mech Eng 346:1021–1050

Wu C, Fang JG, Li Q (2019) Multi-material topology optimization for thermal buckling criteria. Comput Methods Appl Mech Eng 346:1136–1155

Ye HL, Wang WW, Chen N, Sui YK (2017a) Plate/shell topological optimization subjected to linear buckling constraints by adopting composite exponential filtering function. Acta Mech Sinica 32(4):649–658

Ye HL, Wang WW, Chen N, Sui YK (2017b) Plate/shell structure topology optimization of orthotropic material for buckling problem based on independent continuous topological variables. Acta Mech Sinica 33(5):899–911